Video Article

Use of Sacrificial Nanoparticles to Remove the Effects of Shot-noise in Contact Holes Fabricated by E-beam Lithography

Shankar B. Rananavare[1], Moshood K. Morakinyo[2]

[1]Department of Chemistry, Portland State University

[2]Logic Technology Department, Intel Corporation

Correspondence to: Shankar B. Rananavare at ranavas@pdx.edu

URL: https://www.jove.com/video/54551
DOI: doi:10.3791/54551

Keywords: Engineering, Issue 120, E-beam/EUV lithography, electrostatic funneling, resist reflow, plasma etching

Date Published: 2/12/2017

Citation: Rananavare, S.B., Morakinyo, M.K. Use of Sacrificial Nanoparticles to Remove the Effects of Shot-noise in Contact Holes Fabricated by E-beam Lithography. *J. Vis. Exp.* (120), e54551, doi:10.3791/54551 (2017).

Abstract

Nano-patterns fabricated with extreme ultraviolet (EUV) or electron-beam (E-beam) lithography exhibit unexpected variations in size. This variation has been attributed to statistical fluctuations in the number of photons/electrons arriving at a given nano-region arising from shot-noise (SN). The SN varies inversely to the square root of a number of photons/electrons. For a fixed dosage, the SN is larger in EUV and E-beam lithographies than for traditional (193 nm) optical lithography. Bottom-up and top-down patterning approaches are combined to minimize the effects of shot noise in nano-hole patterning. Specifically, an amino-silane surfactant self-assembles on a silicon wafer that is subsequently spin-coated with a 100 nm film of a PMMA-based E-beam photoresist. Exposure to the E-beam and the subsequent development uncover the underlying surfactant film at the bottoms of the holes. Dipping the wafer in a suspension of negatively charged, citrate-capped, 20 nm gold nanoparticles (GNP) deposits one particle per hole. The exposed positively charged surfactant film in the hole electrostatically funnels the negatively charged nanoparticle to the center of an exposed hole, which permanently fixes the positional registry. Next, by heating near the glass transition temperature of the photoresist polymer, the photoresist film reflows and engulfs the nanoparticles. This process erases the holes affected by SN but leaves the deposited GNPs locked in place by strong electrostatic binding. Treatment with oxygen plasma exposes the GNPs by etching a thin layer of the photoresist. Wet-etching the exposed GNPs with a solution of I_2/KI yields uniform holes located at the center of indentations patterned by E-beam lithography. The experiments presented show that the approach reduces the variation in the size of the holes caused by SN from 35% to below 10%. The method extends the patterning limits of transistor contact holes to below 20 nm.

Video Link

The video component of this article can be found at https://www.jove.com/video/54551/

Introduction

The exponential growth in computational power, as quantified by Moore's law[1,2] (1), is a result of progressive advances in optical lithography. In this top-down patterning technique, the achievable resolution, *R*, is given by the well-known Raleigh theorem[3]:

$$R \propto \frac{\lambda}{NA}$$

Here, λ and *NA* are the light wavelength and numerical aperture, respectively. Note that $NA = \eta \cdot sin\theta$, where η is the refractive index of the medium between the lens and the wafer; $\theta = tan^{-1}(d/2l)$ for the diameter, *d*, of the lens, and the distance, *l*, between the center of the lens and the wafer. Over the last fifty years, the lithographic resolution has improved through the use of (a) light sources, including excimer lasers, with progressively smaller UV wavelengths; (b) clever optical designs employing phase-shift masks[4]; and (c) higher *NA*. For exposure in air (η = 1), *NA* is always less than unity, but by introducing a liquid with η >1, such as water[5], between the lens and the wafer, *NA* can be elevated above *1*, thereby improving the resolution of immersion lithography. Currently viable paths to a 20-nm node and beyond include extreme UV sources (λ = 13 nm) or patterning techniques using complex double and quadruple processing of a multilayered photoresist[6,7].

At nanometer-length scales, statistical fluctuations, caused by shot-noise (SN), in the number of photons arriving within a nano-region cause variation in the dimensions of lithographic patterns. These effects are more pronounced with exposure to high-energy EUV light and E-beams, systems that need orders of magnitude fewer photons/particles compared to normal optical lithography[8]. Supersensitive chemically amplified (with a quantum efficiency >1) photoresists also introduce a chemical SN caused by a variation in the number of photoreactive molecules in exposed nanoregions[9,10]. Lower sensitivity photoresists that need longer exposures suppress these effects, but they also reduce throughput.

On the molecular scale, the contribution to line-edge roughness from the molecular size distribution inherent to the photoresist polymers may be reduced by using molecular resists[11]. An approach that is complementary to this top-down processing of nano-patterning is the use of bottom-up methods[12,13] that rely specifically on the directed self-assembly (DSA) of diblock polymers[14]. The ability of these processes to direct nucleation and to create non-uniform spacing between desired patterns, such as holes or lines, remains challenging. The size distribution of

molecular components[15,16] also limits the scale and yield of fabrication[17,18]. Similar problems limit microcontact printing of nanoparticles in soft lithography[19].

This paper presents studies of a new hybrid approach (**Figure 1**) that combines the classic top-down projection lithography with electrostatically directed self-assembly to reduce the effect of SN/line-edge roughness(LER)[20]. Positively charged amine groups on self-assembled monolayers (SAMs) of *N*-(2-aminoethyl)-11-amino-undecyl-methoxy-silane (AATMS) underlying the PMMA film are exposed after development. The negatively charged photoresist film of PMMA electrostatically funnels negatively charged gold nanoparticles (GNPs), capped with citrate,[21-24] into SN-affected holes[25]. Re-flow of the PMMA photoresist engulfs predeposited nanoparticles in the film.

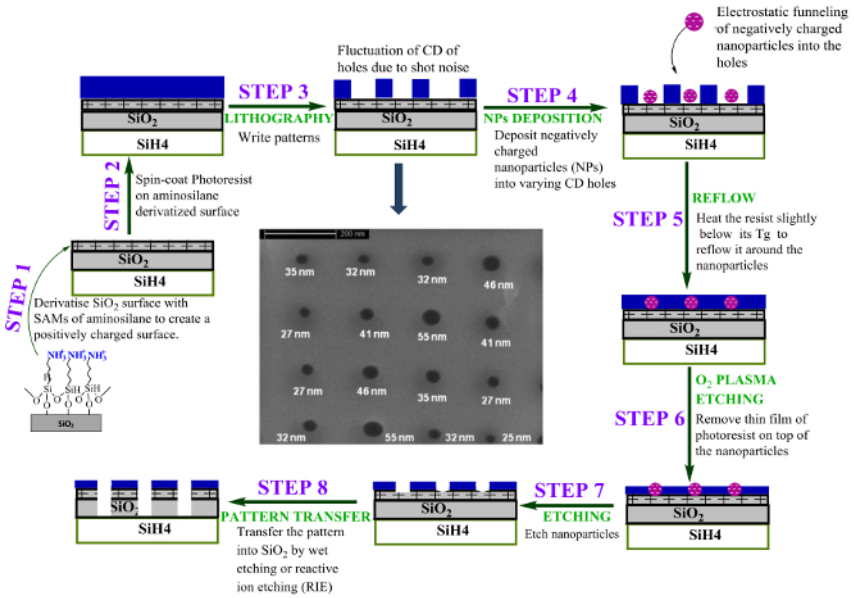

Figure 1: Schematic representation of the strategy to remove the effects of shot-noise and line-edge roughness for the patterning of contact holes using NPs of precise size. Here, the critical dimension (CD) is the desired diameter of the holes. The approach (step 1) begins with depositing a self-assembled monolayer (SAM) of silane molecule bearing positively charged amine groups on the oxide surface of a silicon wafer. Next, E-beam lithography is used to pattern the holes (steps 2 and 3) in PMMA photoresist film, the blue layer, which generates shot-noise, as illustrated in the inset SEM image. Lithography exposes amine groups at the bottom of the holes. Step 4 entails the aqueous phase deposition of controlled-size, citrate-capped (negatively charged) gold nanoparticles (GNPs) in lithographically patterned holes using electrostatic funneling (EF). In step 5, heating the wafer to 100 °C, below the glass transition temperature of the PMMA, 110 °C, causes the reflow of the photoresist around pre-deposited nanoparticles. Etching overlaid PMMA with oxygen plasma (step 6) exposes the GNPs, and subsequent wet-etching (iodine) of the exposed particles (step 7) creates holes corresponding to the size of the GNPs. When coupled with reactive-ion/wet-etching, it is possible to transfer the hole pattern in the photoresist to SiO_2 (step 8)[31]. Reprinted with permission from reference[20]. Please click here to view a larger version of this figure.

The electrostatic interaction between the oppositely charged GNPs and amine groups on the substrate prevents the displacement of the GNPs from the binding site. The reflow step maintains the relative location of the GNPs but erases the holes and the effects of SN/LER. Plasma/wet etching steps regenerate holes that have the size of the GNP. Reactive-ion etching transfers their pattern to SiO_2 hard-mask layers. The method relies on using more uniformly sized nanoparticles than a patterned nanohole (NH), expressed as the standard deviation, σ, such that $\sigma_{GNP} < \sigma_{NH}$. This report focuses on steps (4 and 5 described in **Figure 1**) involving the deposition of nanoparticles from dispersion and the reflow of the photoresist around them to assess the advantages and limitations of the method. Both steps are, in principle, scalable to larger substrates, requiring no extensive modification of the current flow of producing modern integrated circuits on chips.

Protocol

1. Derivatize and Characterize the Surface of the Silicon Wafers

1. Clean the surface of wafers using Radio Corporation of America (RCA) cleaning solutions SC1 and SC2.
2. **Prepare SC1 and SC2 by volumetrically mixing the following chemicals:**
   SC1: H_2O_2:NH_4OH:H_2O = 1:1:5 v/v and SC2: H_2O_2:HCl:H_2O = 1:1:5 v/v.
   1. Immerse the wafer in SC1 for 10 min at 70 °C, and then perform a deionized water wash.
   2. Follow a similar protocol for SC2 (10 min at 70 °C, followed by a wash).
      NOTE: The cleaning procedure removes organic and ionic impurities and generates silanol groups on the silicon oxide surface of the silicon wafers.
3. **Derivatize the surfaces of the silicon wafers with AATMS**

1. Incubate the cleaned silicon wafer in 0.05 M AATMS (prepared in dry toluene) at 80 °C for 20 min. Sonicate for 5 min in a 100 W sonicator at room temperature in pure toluene for 5 min and dry in a stream of nitrogen gas.

4. **Characterize the surfaces of the derivatized silicon wafers**
   1. Measure the contact angle using a goniometer and ImageJ software[25].
   2. Determine the thickness of the films using an ellipsometer (He-Ne laser light source, λ = 632.8 nm, fixed incidence angle of 70°)[25].
   3. Estimate the surface elemental composition by X-ray photoelectron spectroscopy (XPS)[25].

2. E-beam Patterning

1. Spin-coat photoresist (2% poly(methyl methacrylate (PMMA) in anisole) on AATMS- derivatized wafers at 4,000 rpm for 60 s.
2. Prebake the film at 180 °C for 120 s to dry the photoresist film.
3. Measure the photoresist film thickness using an ellipsometer. Ensure that the He-Ne laser light source, λ = 632.8 nm, is fixed at an incidence angle of 70°. Optimize the sample stage to maximize the detector signal using a reflective surface such as silicon wafer. Use the ellipsometer measurement program (GEMP) on the attached PC to measure the photoresist film thickness; it should be about 100 nm.
4. **E-beam exposure:**
   1. Transfer the wafer to a high-vacuum chamber of an E-beam aligner.
   2. Create a poker dot hole pattern using an electron beam (30 kV accelerating voltage, 37 pA beam current) passing through a 10-µm aperture and providing a 24 µC/cm^3 dosage.
   3. Adjust the pattern pitch and dosage as needed to produce a poker dot-type hole-pattern of the desired hole diameter (80 nm) and pitch (200 nm).
   4. Remove the wafer from the E-beam chamber.

5. **Develop the lithographic pattern:**
   1. Begin pattern development in a solution of methyl isobutyl ketone/isopropyl alcohol (MIBK/IPA, 1:3 (v:v)) for 70 s.
   2. Continue to develop further by immersion in IPA for 30 s. Complete the development by washing in deionized water for 30 s. Dry the wafer in a stream of nitrogen gas.

3. Deposition of GNPs into E-beam-patterned Holes

NOTE: Deposition of GNPs in patterned holes employs two different methods.

1. **Immerse pre-patterned wafers in GNP solutions (Method 1).**
   1. Leave the sample in the GNP suspension medium for 24-48 h, depending on the size of the GNP and the diameters of the holes. Use a 20-nm, citrate-capped GNP suspension containing 7.0 x 10^{11} NPs/mL.
      NOTE: One may employ a GNP size from 10-100 nm and a concentration range from 5.7 x 10^{12} - 5.7 x 10^9 NPs/mL, as provided by Ted Pella. Note that the deposition density obeys the diffusion law $\propto (Dt)^{1/2}$, where D and t are diffusion coefficients of the nanoparticle and deposition time, respectively (*i.e.,* smaller particles take a shorter time for deposition, as discussed in reference 20, **Figure 2c**).

2. **Spray-deposit GNPs on the patterned wafers (Method 2)**
   1. To deposit GNPs by evaporation, spray a solution of GNPs onto the patterned substrate, placed horizontally. Orient the hand-held sprayer (Method 2) so that the spray is directed perpendicularly to the substrate surface.
   2. Spray a sufficient volume of the suspension solution to wet the entire substrate surface.
      NOTE: It may be necessary to dilute the GNP suspension by 10x to avoid forcing multiple nanoparticles into a large hole.
   3. Incubate samples on a hot plate maintained at 30-35 °C to produce controlled evaporation for 10 min.

3. After deposition (by either Method 1 or Method 2), mildly ultrasonicate (100 W) the samples in deionized water for 50 s and dry in a stream of nitrogen gas.

4. Scanning Electron Microscopy Imaging

NOTE: Two types of studies involved conventional top-down and cross-sectional SEM imaging.

1. **For top-down SEM images, use an E-beam accelerating voltage of 5 kV at a current of ~300 µA to prevent damage to the photoresist film.**
   Caution: The lowest possible voltage and current setting are necessary to reduce chain scission reactions in the photoresist. These chain scission reactions reduce the glass transition temperature of the polymer, which in turn affects the operational temperature for the resist reflow step described below.
2. **Cross-section imaging:**
   1. Sputter-coat 10 nm of thick gold film over PMMA photoresist to prevent ion-beam damage. Use a focused Ga ion beam operated at 30 kV and 93 pA to cut through the holes. Obtain cross-section SEM images by tilting the wafer from its normal horizontal position.

5. Reflow of PMMA Photoresist around GNPs in the Patterned Holes

1. Heat the patterned substrates on a hot plate at T_{reflow} (100 °C) for 3 min, which is below the pre-determined glass transition temperature, T_g (110 °C), of 950,000 g/mol PMMA; the rate of reflow for the polymer was 1.7 ± 0.1 nm/s.

Caution: Significantly faster reflow occurred for the patterned areas that had previously been exposed to the E-beam during imaging with scanning electron microscopy (SEM), perhaps because of the cleavage of the polymeric backbone chain during exposure to the electron beam, leading to a reduction of T_g. This observation is supported by the studies from Keymeulen and co-workers, who noted that exposure to X-ray radiation reduced the T_g of PMMA[26].

6. Dry- and Wet-etch

1. Dry-etch for sufficient duration (55 s) with oxygen-plasma to expose GNPs covered with a thin film of PMMA after reflow. Carefully monitor the rate of PMMA film etching as a function of time using an ellipsometer or thin film thickness monitor.
   NOTE: A too-short etching duration may not expose the GNPs, while etching for too long would completely remove the PMMA film. For 950 kDa PMMA, the etch rate was 1.5 nm/s, necessitating 55 s of etching time.
2. Wet-etch GNPs at the bottom of the contact holes after reflow using a solution of iodine, containing 1.0 g of iodine crystal (I_2), 4.0 g of potassium iodide (KI), and 40 mL of deionized water, for 10 min.
   NOTE: Potassium iodide improves the solubility of the iodine in solution and facilitates gold etching. The reaction of gold with iodine ($2Au + I_2 \rightarrow 2 AuI$) produces gold iodide, which is slightly soluble in aqueous solution at room temperature.

7 . Calculation of Particle Displacement, Density, and Fill Fraction

1. **Locating the hole center and GNP displacement:**
   1. By hand, draw horizontal and vertical best-fit straight lines through the rows and columns of holes, respectively, to established hole centers at the intersections of these lines (**Figure 2a and 2b**). Include at least 500+ holes in the calculations.
   2. Manually determine the position, *r*, of each nanoparticle relative to the center of the nanohole (*i.e.,* the displacement) where it was deposited (**Figure 2b**).

2. Determine the particle count versus displacement histograms using a standard spreadsheet program.
3. **Calculation of the particle density: ρ = *N* (Number of Particles)/Unit Area (μm^2):**
   1. First, determine the annular area of a ring with a fixed width *(≈R/10,* where *R* is the radius of the hole) and bounded by two radii (r_1, r_2) *at a displacement of r* (=(r_1+r_2)/2); $A = \pi(r_2^2 - r_1^2)$.
   2. Sum the number of particles, *N*, in the area from the histogram constructed in step 7.2, above.
   3. Repeat the procedure as a function of *r* to generate about 10 equal steps terminating at *r* = *R*, the hole radius.

4. Fit the particle density versus the displacement data to a Gaussian curve using a nonlinear least squares procedure (**Figure 2a**, inset)[20]. Extract the standard deviation of displacement ($\sigma_{deposition}$) for the deposition and its fitting uncertainty.
5. Repeat the above procedure for the SEM patterns obtained after the photoresist reflow using an SEM image shown in **Figure 2c**.
   NOTE: After the reflow holes disappear, draw best-fit horizontal and vertical lines on GNP positions to determine the best-fit values for the hole centers. Calculate the particle displacements as in step 7.1 and extract the combined σ_{Total} following the protocol delineated in steps 7.2-7.4.
   NOTE: Here, combined or total refers to the overall displacement of GNP due to the deposition and reflow steps.
6. Determine the fill fraction by estimating the ratio of the number of filled holes to the total number of holes, **Figure 2b**.

Representative Results

Figure 2 shows an SEM image of 20-nm GNPs deposited in 80-nm diameter holes patterned in a 60-100 nm-thick PMMA film driven by electrostatic funneling. As observed by others[22], the process resulted in about one particle per hole. The distribution of particles around the center of the holes was Gaussian (top right inset). Most holes (93%) contained one GNP, and 95% of these particles occurred within 20 nm of the center. Further optimization, discussed elsewhere, is needed to improve the fill-fraction and the centering of the GNPs[20,25]. **Figure 2b** and **2c** shows SEM images of the deposited GNPs from larger regions of the wafer, before and after the reflow of the photoresist. The discussion section presents further quantitative analysis.

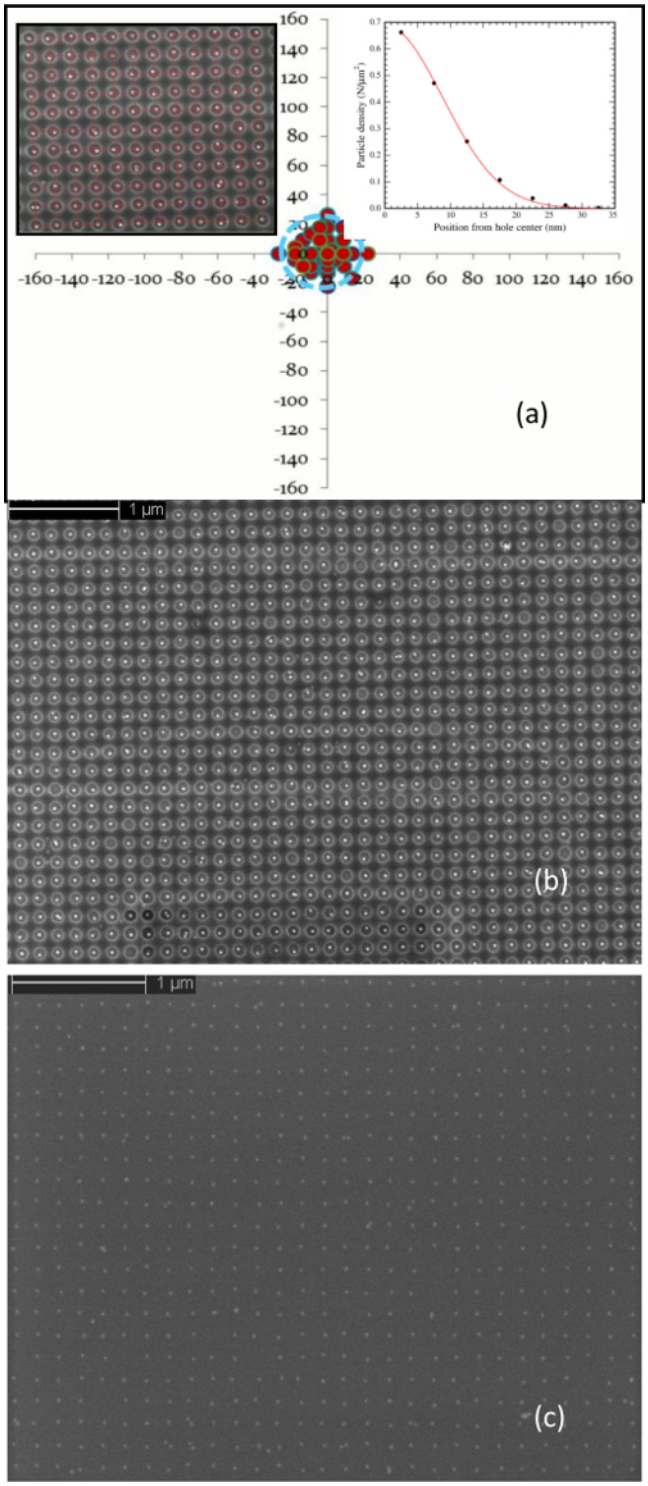

Figure 2: (**a**) 20-nm diameter GNPs deposited in 80 nm diameter holes separated by a pitch, *P*, of 200 nm (top left inset). 93% of the holes contain one nanoparticle, and 95% of the nanoparticles are within 18 nm from the center (blue circle). The top right inset shows a Gaussian distribution of the particle displacement from the center, with σ = 9.0 ± 0.1 nm. (**b**) SEM image of a large area after deposition, σ = 9 ± 1 nm. (**c**) Same as b) after the reflow of the photoresist, σ = 11 ± 2 nm. Modified with permission from reference[20]. Please click here to view a larger version of this figure.

The evaporative deposition could reduce the 24-48 h required for deposition[25]. When dispersions of nanoparticles were allowed to evaporate on the patterned surface, GNPs deposited on the PMMA film, as well as in holes. Mild ultrasonication in a buffered solution removed weakly bound GNPs on the PMMA, leaving only the strongly bound particles in the holes. **Figure 3** illustrates how multiple particles could be forced into holes using this method because of the reduced inter-particle repulsion in the progressively concentrated ionic dispersion. Such ionic screening effects should be avoided, since they allowed multiparticle occupancy and lowered efficiency of the electrostatic funneling that directs the particle to the center of the hole. Lowering the concentration of GNPs in the depositing dispersion, along with ultrasonication, would potentially allow for the deposition of one particle per hole more rapidly than the bulk solution-phase deposition. In this work, we did not optimize the necessary conditions.

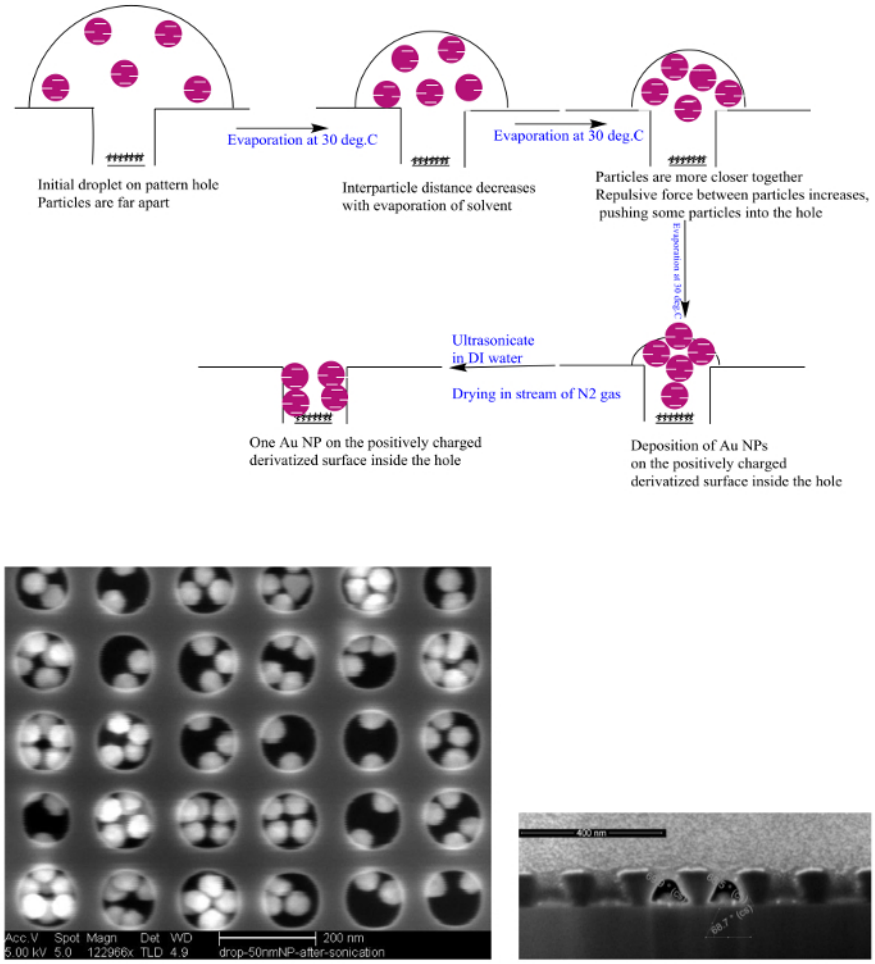

Figure 3: Deposition of GNPs during an evaporation lasting more than 20 min. The bottom SEM micrographs show top-down and cross-sectional views of holes patterned by E-beam. Modified with permission from reference[25]. Please click here to view a larger version of this figure.

The cross-sectional SEM profile displayed the hole sidewalls tilted towards their centers. The angle of the sidewall was less than the optimal 90°, creating an increasing cross-sectional area in the well upon approaching the photoresist-wafer interface. This configuration explains the observed packing pattern (left) of particles, indicating their displacement away from the center of the hole. Better focusing of the E-beam, below the interface between air and the photoresist film, would eliminate such an artifact.

Thin, solid films of PMMA photoresist[27-30] liquefy and flow near the glass transition, T_g, of 110 ºC. A temperature 10° below the T_g of the photoresist polymer, PMMA, initiated a slow reflow of the photoresist. In the softened, liquid-like, glassy state, the surface tension of the photoresist film reduced the edge curvature and roughness, resulting in a suppression of LER effects. The advancing liquid photoresist front completely engulfed nanoholes, along with the deposited GNPs, as illustrated in **Figure 4**, where the number of GNPs per hole was high. Note how the photoresist reflow from the hole borders erased the pattern of nanoholes in the film. Nonetheless, strongly bound GNPs locked into the positional registry of the pattern. Remarkably, these photoresist-reflow studies revealed strong electrostatic binding of the citrate-capped GNPs to amine-terminated silanes. The similarity of the deposition pattern of GNPs before and after reflow supported this conclusion; see **Figure 4c** (*vide infra*).

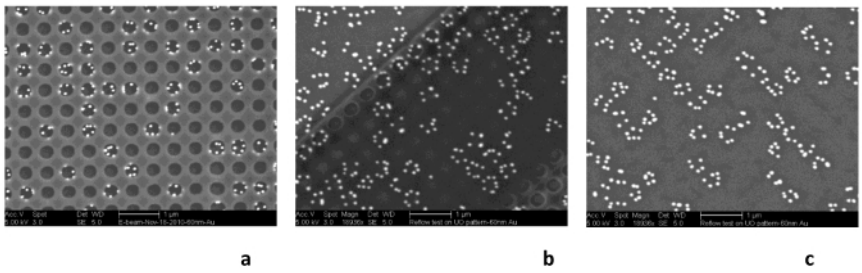

Figure 4: The positions of the deposited GNPs are relatively insensitive to the reflow of the photoresist (see the text). Patterns of the deposited 60 nm GNPs in 250-nm holes: (a) before reflow, (**b**) after partial reflow, and (**c**) after complete reflow. Please click here to view a larger version of this figure.

The overall sequence of steps and the changes occurring in the corresponding SEM images are shown in **Figure 5**. In **Figure 5b**, the holes in the film shrank during photoresist reflow, while the engulfing process was completed in less than 3 min (**Figure 5c**). Oxygen plasma etched the thicker film of photoresist that overlaid on top of GNPs, exposing them to air. Once exposed, these GNPs were wet-etched using gold etching solution based on KI/I_2 (**Figure 5d**). The coefficient of variation for the diameters was 9% for the hole formed by the GNP-assisted process. Note that in these studies, the starting diameter of the holes shrank from 80 to 20 nm, which illustrates the strength of the approach. The primary limitation of the method is the introduction of uncertainty in the position of a recreated hole center due to a combination of uncertainties introduced during the GNP deposition and the resist reflow. Current ongoing work attempts to address these effects. Besides gold, other nanoparticles of different materials, such as silica (etchable in dilute HF), can be used to reduce materials and processing costs. The primary requirement is that the nanoparticle/nanostructure must be selectively etchable without affecting the resist material.

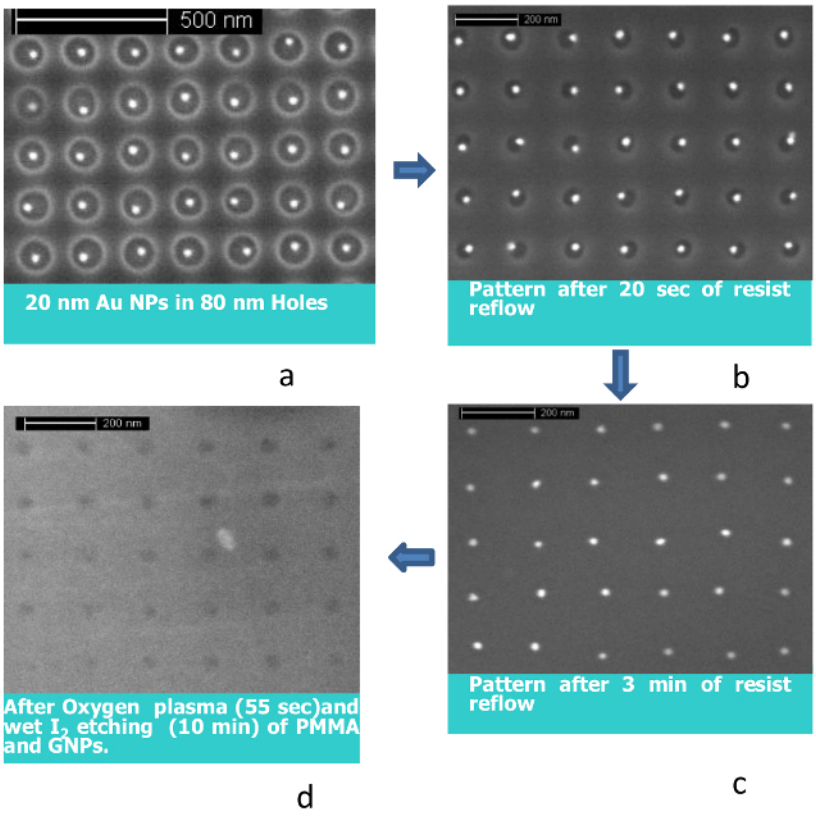

Figure 5: SEM. Images collected during the steps employed to minimize the variation of hole sizes. (**a**) Deposition (24 h). (**b** and **c**) Reflow of the photoresist (20 s, 3 min). **(d**) Etching PMMA (O_2 plasma: 55 s) and GNP (wet-etch with I_2/KI solution: 10 min). Please click here to view a larger version of this figure.

Discussion

Shot-noise (SN) in lithography is a simple consequence of statistical fluctuations in the number of photons or particles (N) arriving in a given nano-region; it is inversely proportional to the square root of a number of photons/particles:

$$SN \propto 1/\sqrt{N} \propto 1/\sqrt{A} \propto 1/r$$

where *A* and *r* are the area and the size of the exposed region, respectively. For example, when using an ArF 193-nm (6.4-eV) excimer laser to pattern 50-nm holes, the number of photons received is approximately 1 x 10^6 at the exposure dose of 52 mJ/cm^2. For a 50 keV E-beam source, the number of electrons delivering 50 mJ/cm^2 would be about 128, implying that the effect of SN would be 100 times greater for E-beam lithography. Furthermore, the number of photons/electrons arriving in a given region decreases directly with the area of the pattern. Consequently, a large fluctuation in the size of holes that received "identical" exposure results occurs as the dimension of the hole to be crafted decreases. For the 35 nm holes shown in **Figure 1** with the 30 keV E-beam, about 1,440 electrons deliver the requisite dose of 24 μc/cm^2. To pattern 20 nm holes under identical conditions, one would need about 400 electrons, which is close to the theoretical SN limit (200 electrons) given by Moreau[32]. Currently, the only way to suppress the effect of SN is through the use of a low-sensitivity photoresist that needs a higher electron/photon dose. It comes at the cost of lower throughput and higher costs for nano-patterning. Our method reduces the effect of size fluctuations by using monodisperse nanostructures to redefine the size of the lithographically patterned holes while maintaining the original positional registry. The registry is fixed by the strong electrostatic binding of nanostructures to the surface, guided by electrostatic funneling.

The success of the patterning in this method depends on two effects. The first is the variation in the sizes of the holes, and the second is the centering of the nanoparticles within the holes that affect the positional registry. The coefficient of variation for the diameter of holes patterned through this approach (9%, or 19 ±2 nm) is comparable to the coefficient of the size (8%) of the GNPs[20]. On the other hand, as revealed in **Figure 1**, the E-beam-patterned 35 nm (35 ±9) holes, made without using this approach, had a CV of 35%. The corresponding CV of E-beam-alone patterning would become even worse when fabricating 20 nm holes. The SN can be set to be proportional to the CV, with rough estimates of CVs for 20 nm and 80 nm holes at 61% and 15%, respectively. The method presented here provides at least a six-fold (~61%/9%) improvement in CV over E-beam-alone patterning of 20 nm holes. Even starting with 80-nm holes, almost 60% improvement in CV results (~15%/9%) occurs after this approach.

The second effect concerns particle deposition away from the geometric center of the holes (registry). Two contributing factors to this effect were extracted from SEM data collected after the deposition of GNPs in holes (**Figure 2b**) and after photoresist-reflow (**Figure 2c**). The statistical analysis of the displacement of GNPs from the center of the nanoholes in which they resided (**Figure 2a**) revealed that during the solution-phase deposition, the distribution of GNPs about the center of the hole was Gaussian, with a standard deviation ($\sigma_{Deposition}$) of 9 nm, or roughly half the diameter of GNPs. The analysis procedure was equivalent to assuming that the particles, on average, remain at the center of holes, although individually they may be displaced randomly due to diffusion during deposition.

The second factor affecting displacement is due to the motion of GNPs during the photoresist reflow. Results, presented in **Figure 4**, indicate that the positively charged AATMS SAM binds so strongly to GNPs that they do not move during the reflow of the photoresist. A similar analysis of SEM images (*vide supra*) collected after the photoresist reflow (**Figure 2c**) step provided the overall standard deviation (σ_{Total}) in the particle positioning (*i.e.,* registry) after the deposition and reflow. To extract the contribution of resist reflow, we assumed that the processes of deposition and photoresist-reflow produce independent effects in displacing particles from the center of holes, such that:

$$\sigma^2_{Total} = \sigma^2_{Deposition} + \sigma^2_{Resist\text{-}reflow}$$

Using the fitted values of $\sigma_{Deposition}$ (9 ±1 nm) and σ_{Total} (11 ±2 nm), the extracted value of $\sigma_{Resist\text{-}reflow}$ was estimated to be 6 nm, which is comparable to three times the standard deviation in the 20 nm GNPs. Such a low standard deviation implies a very negligible effect on the displacement of bound particles during the photoresist reflow process. Nevertheless, the $\sigma_{Deposition}$ appears to vary directly with the size of the GNP; thus, it needs significant improvements. A model presented elsewhere[20] suggests the optimization of the charge-density of the photoresist film and SAM to improve the positional registry. Several methods, including the use of electrostatic bias and charge on GNPs, are currently being explored. Note, as discussed above, that an SEM image analysis provides a straightforward method for the above process of optimization.

The commercial availability of almost monodisperse GNP particles dictated the choice of gold nanoparticles. In principle, other inexpensive nanomaterials, such as silica nanoparticles derivatized with appropriately charged chelant, are also suitable candidates. The primary criterion for the selection of nanoparticles is their monodispersity and their susceptibility to etching. For electrostatic funneling, appropriate complementary charges on the SAM and NP must be present. The charge on NPs depends on its zeta potential, whose sign and magnitude can be tuned either through the pH of the solution or the charge on chelants. Similarly, selecting cationic or anionic terminal end groups allows for the modification of surface charge on the SAM. If perfected, the method readily extends to pattern trench lines with nanowires[33-35]. The overall success of the method will depend on optimizing the placement and filling nanostructures on pre-patterned photoresist films, exploiting electrostatic, magnetic, or ligand-ligation interactions.

Disclosures

The authors have nothing to disclose.

Acknowledgements

Intel Corporation funded this work through grant number 414305, and the Oregon Nanotechnology and Microtechnology Initiative (ONAMI) provided matching funds. We gratefully acknowledge the support and advice of Dr. James Blackwell in all phases of this work. Special thanks go to Drew Beasau and Chelsea Benedict for analyzing particle positioning statistics. We thank Professor Hall for a careful reading of the manuscript and Dr. Kurt Langworthy, at the University of Oregon, Eugene, OR, for his help with E-beam lithography.

References

1. Moore, G. E. Cramming more components onto integrated circuits *Electronics* . **38** (8), 114 (1965).
2. Moore, G. E. Lithography and the future of Moore's law. *SPIE Proc.: Advances in Resist Technology and Processing XII.* (ed. Robert D. Allen) **2438** 2-17 (1995).
3. Rayleigh, L. On the theory of optical images, with special reference to the microscope. *The London, Edinburgh, and Dublin Philosophical Magazine and J. Sci.* **42** (255), 167-195 (1896).
4. Levenson, M. D., Viswanathan, N. S., & Simpson, R. A. Improving resolution in photolithography with a phase-shifting mask. *IEEE Trans. Electron Devices.* **29** (12), 1828-1836 (1982).
5. French, R. H., & Tran, H. V. Immersion Lithography: Photomask and Wafer-Level Materials. *Annu. Rev. Mater. Res.* **39** (1), 93-126 (2009).
6. Borodovsky, Y. Complementary Lithography at Insertion and Beyond in *Complementary Lithography - Stochastics Suppression and EUV, Electronics, Proc. Semicon. West.* June 12, San Franscisco (2012).
7. Reiser, A. Photoreactive Polymers: the Science and Technology of Resists. *John Wiley & Sons.* (1989).
8. Brunner, T. A. Why optical lithography will live forever. *J. of Vac. Sci. & Technol. B: Microelectronics and Nanometer Structures.* **21** (6), 2632-2637 (2003).
9. Tran, H., Jackson, E., Eldo, J., Kanjolia, R., & Rananavare, S. B. in Photochemical reactivity of bis-carbamate photobase generators. *Nanotechnology (IEEE-NANO), 2011 11th IEEE Conference on.* 1683-1688 (2011).
10. Hallett-Tapley, G. L. *et al.* Single component photoacid/photobase generators: potential applications in double patterning photolithography. *J. Mater. Chem. C.* **1**(15), 2657-2665 (2013).
11. Krysak, M., De Silva, A., Sha, J., Lee, J.-K., & Ober, C. K. Molecular glass resists for next-generation lithography. *Proc*. SPIE: *Advances in Resist Materials and Processing Technology XXVI.* (ed. Clifford L. Henderson) **7273** 72732N (2009).
12. Li, M. *et al.* Bottom-up assembly of large-area nanowire resonator arrays. *Nat Nano.* **3** (2), 88-92 (2008).
13. Thiruvengadathan, R. *et al.* Nanomaterial processing using self-assembly-bottom-up chemical and biological approaches. *Rep. Prog. Phys.* **76**(6), 066501 (2013).
14. Tsai, H.-Y. *et al.* Pattern transfer of directed self-assembly (DSA) patterns for CMOS device applications. *Proc.SPIE Advanced Etch Technology for Nanopatterning II.* (eds. Ying Zhang; Gottlieb S. Oehrlein; Qinghuang Lin) **8865** 86850L-86850L (2013).
15. Hawker, C. J., & Russell, T. P. Block Copolymer Lithography: Merging "Bottom-Up" with "Top-Down" Processes. *MRS Bulletin.* **30** (12), 952-966, (2005).
16. Lin, Y. *et al.* Self-directed self-assembly of nanoparticle/copolymer mixtures. *Nature.* **434** (7029), 55-59 (2005).
17. Cheng, J. Y. *et al.* Simple and Versatile Methods To Integrate Directed Self-Assembly with Optical Lithography Using a Polarity-Switched Photoresist. *ACS Nano.* **4** (8), 4815-4823 (2010).
18. Wong, H. S. P., Bencher, C., Yi, H., Bao, X.-Y., & Chang, L.-W. Block copolymer directed self-assembly enables sublithographic patterning for device fabrication. *Proc. SPIE 8323, Alternative Lithographic Technologies IV.* (ed. William M. Tong) 832303-832303-832307 San Hose (2012).
19. Chan, J. C., Hannah-Moore, N., & Rananavare, S. B. Controlled Deposition of Tin Oxide and Silver Nanoparticles Using Microcontact Printing. *Crystals.* **5**(1), 116-142 (2015).
20. Morakinyo, M. K., & Rananavare, S. B. Reducing the effects of shot noise using nanoparticles. *J. Mater. Chem. C.* **3** (5), 955-959 (2015).
21. Cui, Y. *et al.* Integration of Colloidal Nanocrystals into Lithographically Patterned Devices. *Nano Lett.* **4** (6), 1093-1098 (2004).
22. Huang, H.-W., Bhadrachalam, P., Ray, V., & Koh, S. J. Single-particle placement via self-limiting electrostatic gating. *Appl. Phys. Lett.* **93** (7), 073110-073113 (2008).
23. Ma, L.-C. *et al.* Electrostatic Funneling for Precise Nanoparticle Placement: A Route to Wafer-Scale Integration. *Nano Lett.* **7**(2), 439-445 (2007).
24. Richard Bowen, W., Filippov, A. N., Sharif, A. O., & Starov, V. M. A model of the interaction between a charged particle and a pore in a charged membrane surface. *Adv. Colloid Interface Sci.* **81**(1), 35-72, (1999).
25. Morakinyo, M. K., & Rananavare, S. B. Positional control over nanoparticle deposition into nanoholes. *Nanotechnology (IEEE-NANO), 2011 11th IEEE Conference on.* 1677-1682 (2011).
26. Keymeulen, H. R. *et al.* Measurement of the x-ray dose-dependent glass transition temperature of structured polymer films by x-ray diffraction. *J. Appl. Phys.* **102**(1), 013528 (2007).
27. Feng, B. C. *Resist Reflow Method for Making Submicron Patterned Resist Masks.* US patent US4022932 A (1977).
28. You, J.-H. *et al.* Position Shift Analysis in Resist Reflow Process for Sub-50 nm Contact Hole. *Jpn. J. Appl. Phys.* **48**(9), 096502 (2009).
29. Montgomery, P. K. *et al.* Resist reflow for 193-nm low-K1 lithography contacts. *Proc. SPIEAdvances in Resist Technology and Processing XX,* (ed.*Theodore H. Fedynyshyn) Vol.* **5039** 807-816 (2003).
30. King, W. P. *et al.* Atomic force microscope cantilevers for combined thermomechanical data writing and reading. *Appl. Phys. Lett.* **78** (9), 1300-1302 (2001).
31. Chuo, Y. *et al.* Rapid fabrication of nano-structured quartz stamps. *Nanotechnology.* **24** (5), 055304 (2013).
32. Moreau, W. M. in Semiconductor Lithography: Principles, Practices, and Materials. *Springer Science & Business Media.* 419 (2012).
33. Chan, J. C., Tran, H., Pattison, J. W., & Rananavare, S. B. Facile pyrolytic synthesis of silicon nanowires. *Solid-State Electron.* **54** (10), 1185-1191, (2010).
34. Tran, H. A., & Rananavare, S. B. Synthesis and characterization of N- and P- doped tin oxide nanowires. *Nanotechnology (IEEE-NANO), 2011 11th IEEE Conference on.* (2011).

35. Tran, H. A., & Rananavare, S. B. Synthesis and Characterization of n- and p-Doped Tin Oxide Nanowires for Gas Sensing Applications. *Nanoelectronic Device Applications Handbook*. (eds. Krzysztof Iniewski James E. Morris) Ch. 39, CRC Press (2013).